

# Classification of Soil Types Using Hyperspectral Imaging Technology

S Y Jia<sup>1</sup>, H Y Li<sup>1,2</sup>, C X Miao<sup>1</sup> and Q Li<sup>1,\*</sup>

<sup>1</sup> College of Mechanical and Electrical Engineering, China Jiliang University, Hangzhou, PR China

<sup>2</sup> College of Computer Science and Technology, Zhejiang University of Technology, Hangzhou, PR China

Correspondence and email: Q Li, lqdarlbar@163.com

**Abstract.** Soil type is a key indicator in field survey, but the current soil classification method largely depends on personal experiences of operators. In this work, hyperspectral imaging (HSI) technology was applied for the fast and accurate classification of soil types. A total of 183 soil samples collected from Shangyu City, People's Republic of China, were scanned by a near-infrared hyperspectral imaging system with the wavelength range of 874-1734 nm. The soil samples belonged to three major soil types of this area, included paddy soil, red soil and seashore saline soil. The method of successive projections algorithm (SPA) was utilized to select effective wavelengths from the full spectrum. Pattern texture features (energy, contrast, homogeneity and entropy) were extracted from the gray-scale images at the effective wavelengths. The method of support vector machines (SVM) was used to establish classification models. The results showed that: using the combined data sets of effective wavelengths and texture features for modelling reached the optimal correct classification rate of 91.8%. The results indicated that hyperspectral imaging technology could be used for soil type classification, and data fusion combining spectral and image texture information showed advantages for the classification of soil types.

## 1. Introduction

Soil classification is important for soil management and sustainable land utilization [1]. Different soils have different compositions and different environmental and physical properties [2]. At present, Munsell card is the most commonly used soil classification method, which applied soil color to distinguish soil categories. However, this card divides the color space into different small sections, it is not convenient to acquire large amounts of data with modern digital technologies [3]. Meanwhile, this method largely depends on personal experiences, which are easily to cause errors.

Developed from remote sensing, hyperspectral imaging (HSI) has gained extensive attentions from different fields such as food [4], agriculture [5] and medical science [6]. Through each measurement by the HSI instrument, both the spectral information and image texture information of the sample can be obtained. Spectra can reflect the molecular structure and composition of the tested samples. Image texture, which is characterized by the relationship of the intensities of neighboring pixels, has been successfully used for the classification of fruit ripeness [7], fish freshness [8] and

plant disease degree [9]. Cai, et al. used image texture features to classify soil samples with different degrees of salinization, and a higher correct classification rate has been obtained [10]. They considered that when the soil samples were similar in spectral features, texture features would play a positive role in the sample recognition, and combined the information of spectral and texture features can help to improve the classification accuracy. Ma, et al. using HSI technique to distinguish healthy, greening disease infected and zinc-deficient citrus [9]. As the leaf spectra of greening disease infected and zinc-deficient citrus were partially overlapped, and the leaf texture features of greening disease infected and zinc-deficient citrus were similar, utilization of spectral information or texture features for modelling cannot achieve good classification results. However, data fusion combining spectral information and texture features greatly improved the correct classification rate for the three kinds of citrus. To our knowledge, comprehensive utilization of spectral information and image texture features for the classification of soil types was seldom reported.

Hyperspectral image generates an immense amount of data. Some of them may contribute more co-linearity, redundancies, and noise than relevant information to calibration models, which is a huge challenge for the application of HSI technique [11]. Effective wavelength selection, aiming to select only a few wavelengths which carry the most of useful information with minimum collinearity and redundancy from full spectrum, is believed to reduce amount of data, computational task, and build a simple and robust model [12, 13]. Successive projections algorithm (SPA) is a popular tool for wavelength selection in multivariate calibration and classification [14]. It is able to select a small representative set of spectral wavelengths with a minimum of collinearity. In machine visual systems, the most popular method for texture feature analysis is Gray level co-occurrence matrix (GLCM) method [15]. GLCM, created through calculating how often a pixel with a particular gray level value occurs at a specified distance and angle from its adjacent pixels, is able to take into account the specific position of a pixel relative to another. In this work, SPA and GLCM were adopted to select effective wavelengths and extract texture features, respectively.

The objective of this work was to investigate the feasibility of classifying soil types using HSI technique. The specific objective was to build classification models for soil types in utilization of spectral information and image texture features.

## 2. Materials and methods

### 2.1. Soil samples and laboratory reference measurement

Total 183 soil samples sampled from the upper soil layer (0-30 cm) of Shangyu City, Zhejiang province, People's Republic of China, were used in this study. All the samples were air dried and sieved with a diameter of 1 mm. Then they were air dried again at 60°C for 48 h. A small portion of each sample was sent to the agricultural testing center of Zhejiang Provincial Academy of Agricultural Sciences (ZPAAS) for soil classification analyses. The remaining samples were used for HSI measurement.

According to the classification and codes for Chinese soil (National standard of China, GB/T 17296-2009), the soil samples belonged to three major soil types of this area, namely, paddy soil (84 samples), red soil (57 samples) and seashore saline soil (42 samples).

### 2.2. Hyperspectral image acquisition

The hyperspectral images of soil samples were captured by a near-infrared HSI system with the wavelength range of 874-1734 nm and 256 bands. The system was composed of an imaging spectrograph (ImSpector N17E; Spectral Imaging Ltd., Oulu, Finland), a CCD camera (Xeva 992; Xenics Infrared Solutions, Leuven, Belgium), two 150W quartz tungsten halogen lamps (Fiber-Lite DC950 Illuminator, Dolan Jenner Industries Inc., USA), and a conveyer belt which was driven by a stepper motor for sample movement (Figure 1). The entire system was fixed in a darkroom. The soil

samples were put into petri dishes with a diameter of 60 mm. The petri dishes were placed on the conveyer belt for image acquisition. Hyperspectral image provided both spectral and image information simultaneously. Each pixel within the hyperspectral image contained a spectrum at the spectral range of the system, and there was a gray-scale image at each wavelength.

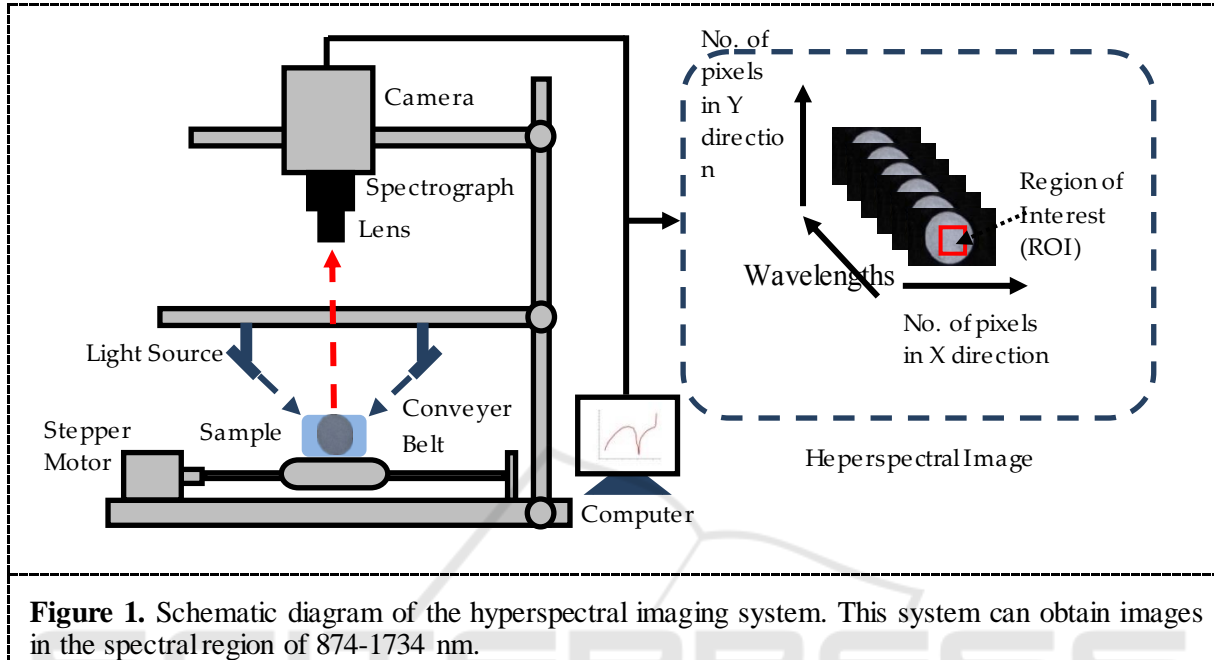


**Figure 1.** Schematic diagram of the hyperspectral imaging system. This system can obtain images in the spectral region of 874-1734 nm.

To acquire clear and non-deformable hyperspectral images, the moving speed of the conveyer belt, the exposure time of the camera, and the height between the lens of the camera and the sample were set as 24 mm/s, 3 ms, and 30.8 cm, respectively.

Raw hyperspectral image ( $I_0$ ) was corrected by white (W) and dark (D) reference images. The white reference image was obtained using a standard Teflon tile (~99.9% reflectance), and the dark reference image was acquired by turning off the light source and covering the camera lens with its opaque cap. The corrected image (I) was calculated by the following equation:

$$I = \frac{I_0 - D}{W - D} * 100\% \quad (1)$$

### 2.3. Spectral data extraction and effective wavelength selection

For each soil sample's hyperspectral image, the region that covered the petri dish without the edge was selected as the region of interest (ROI). The reflectance values of all pixels in the ROI were averaged to generate only one mean spectrum. Then, the mean spectrum was reduced to 975-1645 nm to eliminate noise at edges, which was used to represent the spectral data of one sample. The same procedure was repeated for all ROI images, and a full spectrum matrix 237 samples  $\times$  200 bands was constructed.

Effective wavelengths were selected by the SPA method. The best variable subset was determined on the basis of the root mean square error of leave-one-out cross validation in the calibration set (RMSECV). A detailed description of SPA can be found in literature [16,17].

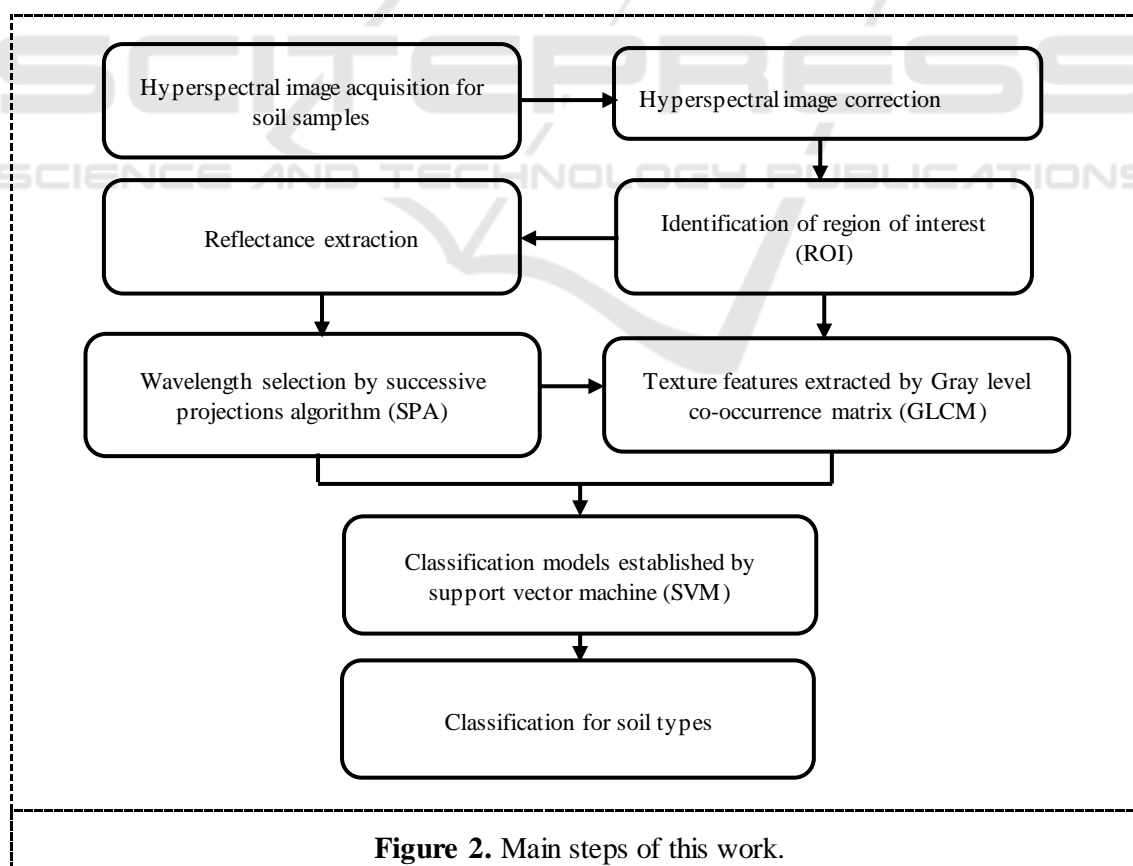
### 2.4. Texture variable extraction

In creating the GLCM, the direction of 0°, 45°, 90° and 135° and distance of one pixel were applied, and four popular texture variables, such as energy, contrast, homogeneity and entropy were

calculated in each direction based on GLCM [18,19]. The mean values of the four directions were used, and four averaged texture variables were obtained from the ROI of one gray-scale image. As the hyperspectral image contained gray-scale images at continuous wavelength bands, a total of 200 gray-scale images have been obtained from a single measurement of one soil sample. Extracting texture features from each gray-scale image would generate a large amount of redundant information which was not useful for modelling. Hence, texture features were only extracted from the gray-scale images at effective wavelengths.

### 2.5. Establishment of classification and regression models

The main steps of the work were shown in figure 2. After hyperspectral image acquisition, correction and reflectance extraction, the samples of each soil type were randomly split into the calibration set and prediction set at a ratio of 2:1 so as to establish classification models: the calibration set was composed of 56 paddy soil samples, 38 red soil samples and 28 seashore saline soil samples, while the prediction set included the remaining 28 paddy soil samples, 19 red soil samples and 14 seashore saline soil samples. Then the method of SPA was used to select effective wavelengths based on the calibration set. The reference data  $y$  in SPA was category value. The samples of paddy soil, red soil and seashore saline soil were assigned category values of 1, 2 and 3. After effective wavelength selection, texture features were extracted by GLCM. The method of support vector machines (SVM) was used to establish classification models based on the effective wavelengths and texture features. SVM has been proved as a reliable method for classification, dealing with both linear and nonlinear data efficiently [20, 21]. In this work, radial basis function kernel was selected as the kernel function, which is the typical general-purpose kernel.



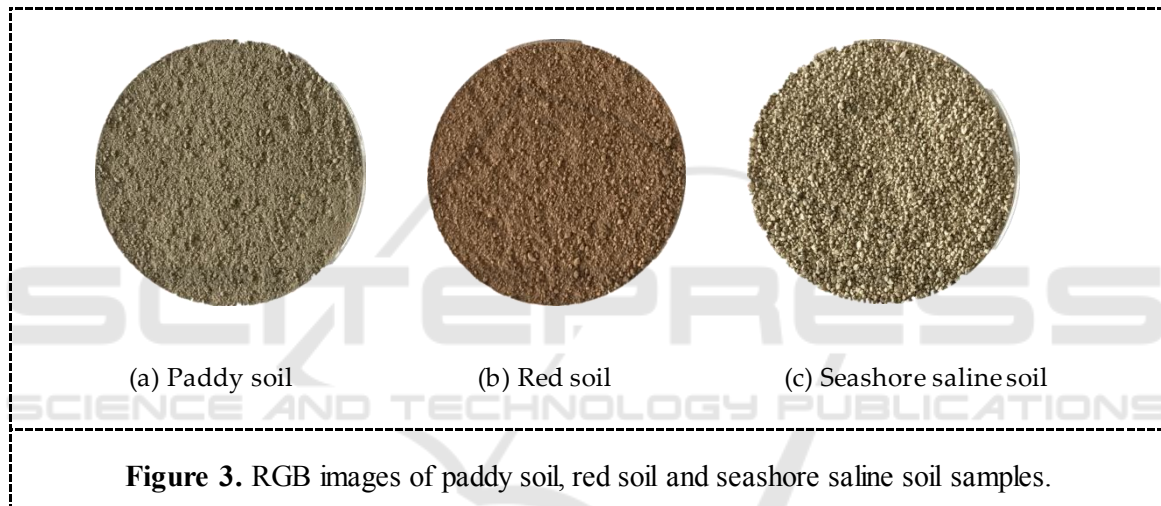
## 2.6. Software

The hyperspectral image analysis was conducted on ENVI 4.6 (ITT, Visual Information Solutions, Boulder, CO, USA) and Matlab 2010 (The Math Works, Natick, MA, USA). The methods of SVM, SPA were operated in Matlab 2010 .

## 3. Results and discussion

### 3.1. Spectral profiles

Figure 3 showed the RGB images of three soil type samples. It can be noted that the surface of seashore saline soil was rougher than that of paddy soil and red soil. As can be seen in figure 4 (a), the average spectrum of each soil type in the range of 975-1645 nm showed similar trend. The significant peaks around 1400 nm appeared in all spectra, which were attributed to the absorption of water in soil. There were some differences in the average spectral baselines. The reflectance value of seashore saline soil was lower than that of paddy soil and red soil, mainly because the light scattering of the surface of seashore saline soil was too intense.



In order to examine the structure of the spectral data, a principal components analysis was performed on the full spectrum matrix. The principal components analysis scores were submitted to Fisher's linear discriminant analysis (LDA). Because the first four principal components (PCs) of the spectral data can explain nearly 100% of total variance, they were set as input of LDA. Figure 4 (b) showed the samples of paddy soil, red soil and seashore saline soil distinguished by the score plot of Fisher's LDA. The correct classification percentage was 85%. It can be observed that the samples of paddy soil and seashore saline soil were relatively well grouped, while some red soil samples were mixed with the samples of the other two soil types.

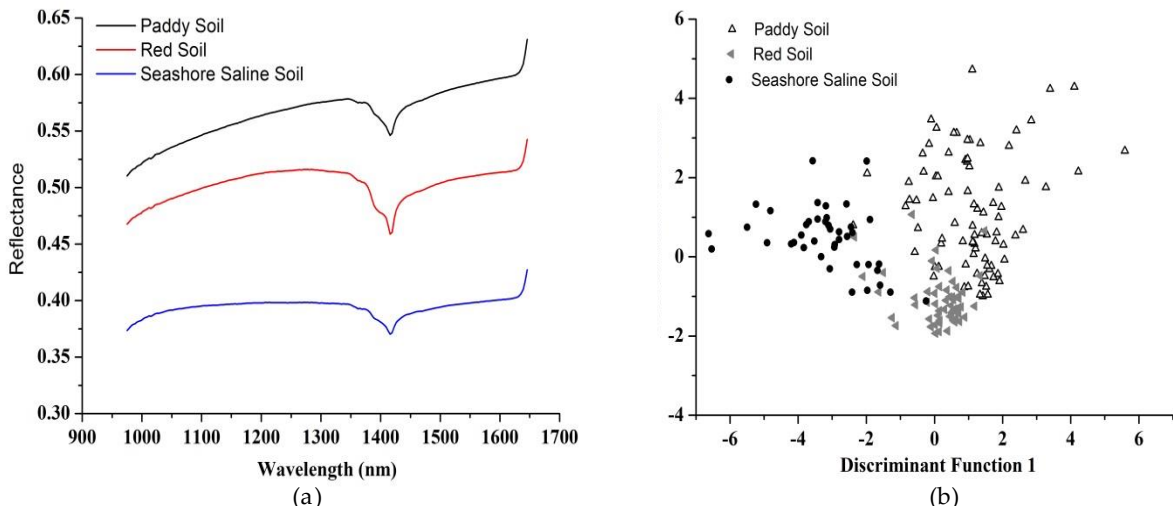


**Figure 4.** (a) The average spectrum of each soil type in the wavelength range of 975-1645 nm ; (b) Grouping of 183 soil samples based on Fisher's LDA using the first four principal components of full spectrum matrix as input.

### 3.2. Effective variables selection

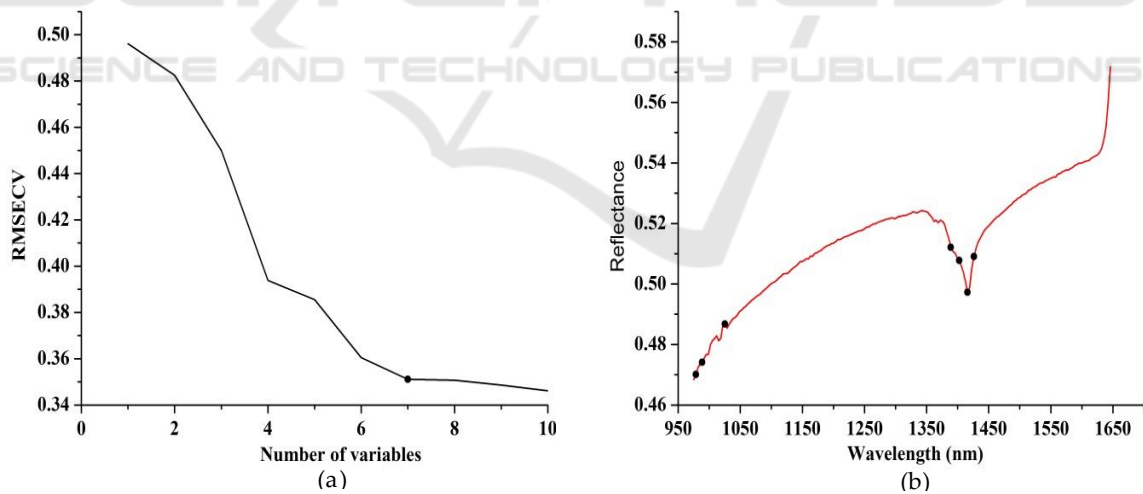


**Figure 5.** RMSECV curves with the number of variables selected by SPA for soil type classification (a). The reference data in SPA was category value. The selected variables (shown as dots) corresponding to raw spectra were presented in (b).

SPA was carried out to select effective variables from the full spectrum. The variation of RMSECV with the number of selected variables for soil type classification is shown in figure 5 (a). Let RMSECVmin be the minimum value in the RMSECV sequence. Seven variables were selected through comparison of the RMSECV values which was not significantly larger than RMSEVmin by

applying the F-test criterion with a significance level  $\alpha=0.25$  [22]. Figure 5 (b) presented an overview of the selected variables corresponding to raw spectra. The selected variables around the peak of 1400 nm can be approximately attributed to the absorption of water absorptions in the second overtone region, while the variables selected in the wavelength range of 950-1050 nm were related to overtones of aromatics C-H bond and amine N-H bond in organics [23]. This indicated that considerable differences existed in moisture content and organic ingredients among the samples of the three soil types.

### 3.3. Texture features extraction and analysis

ROI was defined as a rectangular area in the middle of the sample with 50\*50 pixels (Figure 1). Four texture features (Energy, contrast, homogeneity and entropy) based on GLCM at 7 effective wavelengths were extracted, resulting in a total of 28 texture features (4 texture features  $\times$  7 wavelengths) obtained from the ROIs for each soil sample.

Figure 6 showed the mean values of the four texture features from different soil types. It can be seen that energy and homogeneity of seashore saline soil was highest compared with the other two soil types at the effective wavelengths, which indicated that the image texture of seashore saline soil was rougher than that of the other two soil types [10]. The similar conclusion could be also obtained by analyzing the mean values of contrast and entropy. They were the lowest for seashore saline soil, which meant that the image texture of seashore saline soil contained less local variations. In general, the texture features of seashore saline soil were clearly distinguished from those of the other two soil types, and there were no intersections between the texture features of paddy soil and red soil, although they were close at some effective wavelengths. Hence, it was possible for soil type classification based on these statistics.





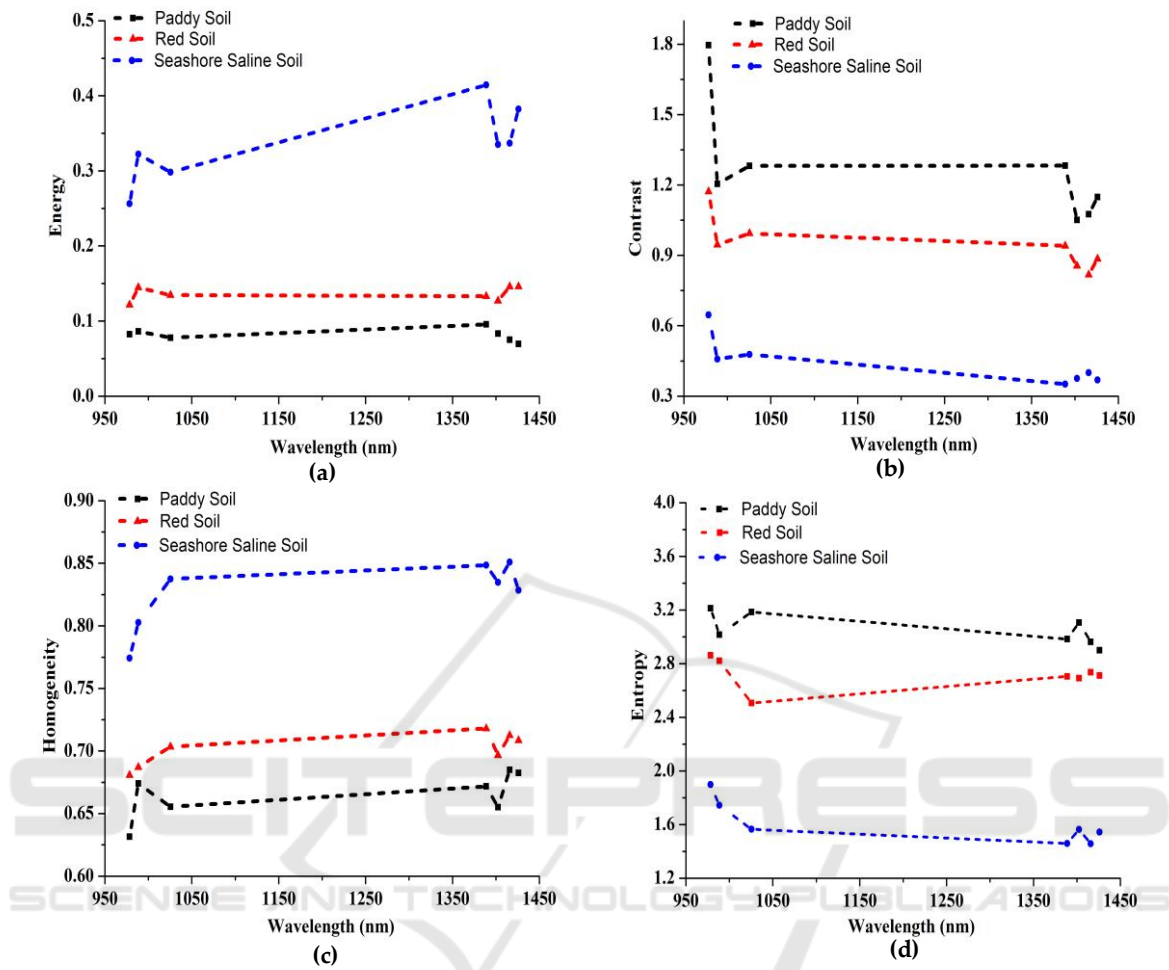


**Figure 6.** The mean texture features of different soil types at the effective wavelengths.

### 3.4. Classification for soil types

To build SVM models for soil type classification, the samples of paddy soil, red soil and seashore saline soil were assigned category values of 1, 2 and 3. Table 1 showed the classification results of SVM models using different input variables. When using spectral effective wavelengths for modelling, it can be note that the discrimination accuracy was 88.5% for the calibration set and 83.6% for the prediction set. The results were similar with the classification performed on the full spectrum matrix by LDA. Then, texture features were used for modelling. The discrimination accuracy was 82.7% for the calibration set and 77.0% for the prediction set. The performances were poorer compared with the model established by effective wavelengths. However, the samples of seashore saline soil were well classified from the samples of the other two soil type.

Finally, both effective wavelengths and texture features were set as input for building SVM models. As can be seen, the discrimination accuracy of the calibration set and prediction set were both improved compared with the models using spectral effective wavelengths or texture features as input. The samples of paddy soil and seashore saline soil were successfully classified, while some samples of paddy soil and red soil were misclassified, and a few seashore saline soil samples were



misclassified as red soil samples. The results indicated that data fusion of combining effective wavelengths and texture features showed advantages for the classification of soil types.

**Table 1.** Classification results for soil types using SVM models established based on different input variables.

Input variables	(c,g) <sup>a</sup>	Calibration set				Prediction set					
		1	2	3	Accuracy	1	2	3	Accuracy		
Effective wavelengths	(23.12, 2.42)	1	51	4	1	91.1%	1	24	2	2	85.7%
		2	3	33	2	86.8%	2	2	16	1	84.2%
		3	0	4	24	85.7%	3	1	2	11	78.6%
		total				88.5%					83.6%
Texture features	(90.95, 0.26)	1	47	9	0	83.9%	1	23	5	0	82.1%
		2	10	27	1	71.1%	2	7	12	0	63.1%
		3	1	1	26	92.8%	3	1	1	12	85.7%
		total				82.7%					77.0%
Effective wavelengths and texture features	(190.12, 2.28)	1	54	2	0	96.4%	1	27	1	0	96.4%
		2	3	34	1	89.4%	2	3	16	0	84.2%
		3	0	1	27	96.4%	3	0	1	13	92.8%
		total				94.2%					91.8%

<sup>a</sup>(c, g) were the parameters of SVM model, c was the penalty coefficient, and g as the kernel function parameter.

#### 4. Conclusions

In this work, a HSI system covering the spectral range of 874-1734 nm was used to classify soil types. The method of SPA was applied to select effective wavelengths from the full spectrum, and texture features of energy, contrast, homogeneity and entropy were extracted from the gray-scale images at the effective wavelengths. The classification models for soil types were established by the method of SVM. The results showed that:

i. The classification model established by the combining data of effective wavelengths and texture features achieved the optimal results for the classification of red, paddy and seashore saline soil compared with the models established by the effective wavelengths or texture features. The correct classification rate was 91.8 %.

ii. The overall results indicated that it was helpful to use image texture features for soil type classification, and HSI technique could be used for soil type classification.

In future work, more soil samples with a wide range of soil types should be studied to build more robust soil type classification models.

#### Acknowledgments

This work was supported by the Natural Science Foundation of Zhejiang Province, China (project no LQ16F010006), the scientific research project of the education department of Zhejiang Province (project no Y201533855 and Y201737559), and the key research and development plan of Zhejiang Province (project no 2018C03040). The authors declare no conflict of interest.

#### Reference

- [1] Hartemink A E and J Bockheim G 2013 *Catena* 104 251-256
- [2] Viscarra Rossel R A, Minasny B, Roudier P and McBratney A B 2006 *Geoderma* 133 320-337
- [3] Meyer R R and Kirkland A 1998 *Ultramicroscopy* 75 23-33
- [4] Zhang C, Guo C, Liu F, Kong W, He Y and Lou B 2016 *J. Food Eng.* 179 11-18

- [5] Gomez C, Gholizadeh A, Borůvka L and Lagacherie P 2016 *Geoderma* 276 84-92
- [6] Neittaanmaki-Perttu N, Gronroos M, Tani T, Polonen I, Ranki A, Saksela O and Snellman E 2013 *Laser Surg. Med* 45 410-7
- [7] Wei X, Liu F, Qiu Z, Shao Y and He Y 2013 *Food Bioprocess Tech.* 7 1371-1380
- [8] Zhu F, Zhang D, He Y, Liu F and Sun D W 2012 *Food Bioprocess Tech.* 6 2931-2937
- [9] Ma H, Ji H and Won S L 2016 *Spectrosc. Spect. Anal.* 36 2344-2350
- [10] Cai S, Zhang R, Liu L and Zhou D 2010 *Math. Comput. Model.* 51 1319-1325
- [11] Dai Q, Cheng J H, Sun D W, Zhu Z and Pu H 2016 *Food Chem.* 197 257-265
- [12] Li J, Tian X, Huang W, Zhang B and Fan S 2016 *Food Anal. Method.* 9 3087-3098
- [13] Mollazade K 2017 *Food Anal. Method.* 10 2734-2754
- [14] Galvão R K H, AraMC Uújo , Fragoso W D, Silva E C, JoséG E, Soares S F C and Paiva H M 2008 *Chemometr. Intell. Lab.* 92 83-91
- [15] Haralick R M, Shanmugam K and Dinstein I h 1973 *Ieee Trans. Syst.* 3 610-621
- [16] Ye S, Wang D and Min S 2008 *Chemometr. Intell. Lab.* 91 194-199
- [17] Insausti M, Gomes A A, Cruz F V, Pistonesi M F, Araujo M C, Galvao R K, Pereira C F and Band B S 2012 *Talanta* 97 579-83
- [18] Mendoza F and Aguilera J M 2004 *J. Food Sci.* 69 E471-E477
- [19] Xie C, Shao Y, Li X and He Y 2015 *Sci. Rep.* 5 16564
- [20] Li S X, Zhang Y J, Zeng Q Y, Li L F, Guo Z Y, Liu Z M, Xiong H L and Liu S H 2014 *Laser Phys. Lett.* 11 065603
- [21] Langeron Y, Doussot M, Hewson D J and Duchêne J 2007 *Eng. Appl. Artif. Intel.* 20 415-427
- [22] Jia S, Yang X, Zhang J and Li G 2014 *Soil Sci.* 179 211-219
- [23] Rossel R A V and Behrens T 2010 *Geoderma* 158 46-54

SCITEPRESS  
SCIENCE AND TECHNOLOGY PUBLICATIONS